HAL open science

Hygromechanical properties of grenadilla wood (Dalbergia melanoxylon)

Ahmad Alkadri, Delphine Jullien, Olivier Arnould, Eric Rosenkrantz, Patrick Langbour, Louise Hovasse, Joseph Gril

To cite this version:

Ahmad Alkadri, Delphine Jullien, Olivier Arnould, Eric Rosenkrantz, Patrick Langbour, et al.. Hygromechanical properties of grenadilla wood (Dalbergia melanoxylon). Wood Science and Technology, 2020, 10.1007/s00226-020-01215-z . hal-02927145

HAL Id: hal-02927145

https://hal.science/hal-02927145v1

Submitted on 1 Sep 2020

HAL is a multi-disciplinary open access archive for the deposit and dissemination of scientific research documents, whether they are published or not. The documents may come from teaching and research institutions in France or abroad, or from public or private research centers.

L'archive ouverte pluridisciplinaire **HAL**, est destinée au dépôt et à la diffusion de documents scientifiques de niveau recherche, publiés ou non, émanant des établissements d'enseignement et de recherche français ou étrangers, des laboratoires publics ou privés.

Hygromechanical properties of grenadilla wood (*Dalbergia melanoxylon*)

Ahmad Alkadri[1,2] · Delphine Jullien[2] · Olivier Arnould[2] · Eric Rosenkrantz[3] · Patrick Langbour[4] · Louise Hovasse[1] · Joseph Gril[5]

Abstract

Grenadilla wood (*Dalbergia melanoxylon* Guill. & Perr.) is a hardwood species found in Tanzania, Mozambique, and other countries in the tropical part of Africa, especially in the Eastern-Central region. Thanks to its high density and good hygroscopic stability, it is used in the making of various musical instruments and fine furniture. Due to the scarcity of published data on this wood species, more studies on its properties are needed to improve its processing and use, and even to search for sustainable alternative materials as its trade is increasingly limited by new regulations. This work is focused on the hygromechanical properties, which hold an important role in the applications of this wood: diffusion coefficients and adsorption–desorption curve (both measured at $T = 20\,°\mathrm{C}$), swelling–shrinkage coefficients and full orthotropic elastic constants using an ultrasonic method. Results show that grenadilla wood possesses small water diffusion coefficients (from $1.54 \pm 0.49 \times 10^{-7}\,\mathrm{cm^2/s}$ in T direction to $4.58 \pm 0.84 \times 10^{-7}\,\mathrm{cm^2/s}$ in L direction), which is probably related to its high density ($1250.0 \pm 26.2\,\mathrm{kg/m^2}$); unique equilibrium moisture content (sorption) curve with a lower fiber saturation point (0.173 ± 0.003); smaller swelling–shrinkage coefficients (0.20 ± 0.03 and 0.32 ± 0.05 in T and R directions, respectively); and elastic constants lower in the longitudinal direction (15.56 ± 1.79 GPa) and higher in the transverse ones (5.10 ± 0.46 GPa and 4.05 ± 0.35 GPa in R and T directions, respectively) than what could be expected with a standard model based on the density only. Several explanations were described here, from the effects of a high extractive content to the possibility of a high microfibril and/or fiber angle.

List of symbols

L	Longitudinal direction
R	Radial direction
T	Tangential direction
c	Diffusing concentration

c_i	Initial diffusing concentration
c_f	Final diffusing concentration
M_t	Total change of moisture content at a given time t
M_f	Total final change of moisture content
$[C]$	Stiffness matrix
C_{ij}	Component of stiffness matrix
$[S]$	Compliance matrix, where $[C] = [S]^{-1}$
DL	A code designating a diffusion sample for L direction
DR	A code designating a diffusion sample for R direction
DT	A code designating a diffusion sample for T direction
D	Coefficient of diffusion, written here as cm^2/s
$[D]$	Matrix of diffusion coefficients, which consists of D for diffusion in L, R and T
D_0	Constant diffusion coefficient D
D_{lin}	Coefficient of diffusion whose values vary linearly with W
D_e	Coefficient of diffusion whose values vary exponentially with W
EMC	Equilibrium moisture content (without unit)
γ	Swelling–shrinkage coefficient (without unit)
$\gamma_{\mathrm{R}}, \gamma_{\mathrm{T}}$	Swelling–shrinkage coefficient for R and T directions, respectively
Γ_V	Volume swelling coefficient
S	A code designating a sample as a swelling–shrinkage sample
α, ϕ	Intrinsic thermodynamic full-cycle curve parameters (unitless)
A, β, K	Empirical partial-cycle curve parameters (unitless)
V	Volume (m^3)
V	Wave propagation velocity (m/s)
V_θ	Wave propagation velocity measured at angle θ (m/s)
W	Water/moisture content of wood (unitless)
W_s	Fiber saturation point of wood (unitless)
W_t	Moisture content of wood sample at time t, Eq. 12
W_i	Initial moisture content (unitless), Eqs. 3, 4 and 12
W_f	Final moisture content (unitless), Eqs. 3, 4 and 12
ζ_x	Hydric capacity of the isothermal envelope for adsorption or desorption, Eq. 7
h	Relative humidity or RH (unitless)
h_i	Initial relative humidity (unitless), referred to Eqs. 3–4
h_f	Final relative humidity (unitless), referred to Eqs. 3–4
m	Mass in g
p, b	Empirical constants to be estimated (no unit), referred to in Eq. 15
μ	Mean values
δ	Standard deviation values
k	Empirical constant to be estimated (no unit) from Eq. 16
l	Thickness of the sample (mm).
ρ	Density of the wood ($\mathrm{kg/m}^3$)
T	Temperature (°C)
h	Relative humidity (unitless)
X	Half-thickness of wood sample used in the diffusion experiments (mm)

Y	Dimension of the sample in particular direction (can be in R, L or T), in mm.
Y_i	Initial dimension of the sample in particular direction, in mm, measured at W_i
Y_f	Initial dimension of the sample in particular direction, in mm, measured at W_f
ϵ	Mechanical or hygroscopic strain of wood
ξ	The weighed parameter for partial-cycle curve, referred to Eqs. 3–6
ξ_a	The weighed parameter for partial-cycle curve during adsorption ($h_f > h_i$)
ξ_d	The weighed parameter for partial-cycle curve during desorption ($h_f < h_i$)
sse	Sum of squared error

Introduction

Grenadilla (*Dalbergia melanoxylon*) is a tree species from the Leguminosae (Fabaceae) family (Détienne 1990; Gérard et al. 2017). It grows in the tropical, savanna part of Africa, and can be found most in Eastern-Central African countries such as Tanzania and Mozambique (Détienne 1990; Malimbwi et al. 2000; Ball 2004; Gérard et al. 2017). The tree can reach a height of 7–10 m, and the leaves are broad with compound form (Chave et al. 2009; Parr et al. 2014).

Grenadilla heartwood, in contrast to its sapwood, is deeply dark in color, which explains its other name: African blackwood. With an air-dry density of its heartwood ranging between 1100 and 1400 kg/m^3, it is one of the woods with the highest density among all commercial timbers in the world (Zadro 1975; Gérard et al. 2017; Sproßmann et al. 2017; Liu et al. 2020). Additionally, it possesses a high extractive content, up to 16 to 25% (Jankowska et al. 2016; Gérard et al. 2017; Yin et al. 2018), many of them from the category of neoflavanoids (Donnelly et al. 1975). These extractives possibly contribute to its high hygroscopic stability—which, however, remains to be proved through meticulous testing—and natural durability against timber-decaying organisms (Hillis 1971; Van Heerden et al. 1980; Rowell and Banks 1985; Gérard et al. 2017). As a consequence, it is used for a lot of applications.

Grenadilla wood is often used for the making of musical instruments such as oboe and clarinet which demands a high-dimensional stability and low roughness during the machining process and the usage (Zadro 1975). Another example on its use in the domain of the musical instrument is in the making of guitar necks, specifically its fret or top part (Sproßmann et al. 2017). Other uses include the making of luxury furniture, ranging from tables and sofas to cabinets (Lancaster and Espinoza 2012; Ogawa 2018) or artworks such as marqueteries. Actually, it was because of this last application that, for years, rising demands of *Dalbergia melanoxylon* have been coming especially from China (Wenbin and Xiufang 2013). Such demands are so high that it has put pressure on the grenadilla stock in the nature and in the market (IUCN 1998; Lancaster and Espinoza 2012; Ogawa 2018).

In 2017, CITES added grenadilla wood, together with all other wood species from the *Dalbergia* genus, to its appendix of endangered species (Snel et al. 2018). Such a decision was justified by the ever-increasing pressure of the demand

of this wood, insufficiently compensated by plantation efforts: Grenadilla is a slow-growing tree species, with time needed to reach mature size ranging from 50–80 to 70–100 years (Malimbwi et al. 2000; Ball 2004). This has led to a decrease in supply, while demand is increasing. Simply raising the timber price would not solve that problem because of the lack of data and regulations, plus inefficient enforcements by laws leading to much illegal trade (Innes 2010; Treanor 2015; Randriamamonjy et al. 2016; Remy 2017).

Today, thanks to the efforts of many stakeholders, grenadilla wood, alongside its *Dalbergia* cousins, is getting the attention it deserves. Laws and tools are being prepared to better regulate the trade flow of these timber species (Hassold et al. 2016; Lowe et al. 2016; Siriwat and Nijman 2018; Ugochukwu et al. 2018). Although recent development has exempted musical instrument making from the *Dalbergia* trade restriction, the still increasing interest in grenadilla also highlights, perhaps unintendedly, the gaps in the literature regarding the species, especially on its precise stock in nature and its material properties. Current efforts are focused on its conservation in nature, thereby closing the gap of knowledge on the stock data. However, material property data remain insufficient. Such knowledge is particularly needed in the context of decreasing availability and stable or increasing demand, where a wiser use of the material is essential. In addition, there is the possibility of a search for substitute material, wood or synthetic, for its many applications.

Related to the needs for products in long-term use, hygromechanical behavior is a key property. As a hygroscopic material, wood exchanges water with its environment to reach an equilibrium state, following a function of surrounding relative humidity (h) and temperature (T) (Hailwood and Horrobin 1946) which results in equilibrium moisture content (EMC) and hygroelastic expansion (swelling or shrinkage). The time-dependent mechanical response of wood is affected by these changes and known as hygromechanical behavior. Although many studies have been conducted on the hygromechanical properties of wood from tropical regions, particularly those of Africa—such as African whitewood, frake and grenadilla's twin wood species in appearance, ebony (Jannot et al. 2006; Fernández et al. 2014; Simo-Tagne et al. 2016a, 2019)—few have determined such properties for grenadilla.

Thus, the objective of this paper is to present the data for the basic properties of grenadilla wood, particularly regarding sorption, diffusion, anisotropic expansion and elasticity. The study of time-dependent behavior and hygromechanical couplings will be left for further investigations.

Materials and methods

Sampling plan

Sampling for hygroscopic characterization

A major part of this study consists of experimental characterizations of diffusion, adsorption and desorption properties of grenadilla. Taking into account the

orthotropical properties of wood, a sampling plan adapted from another study (Olek and Weres 2007) was prepared as follows:

(a) *Material selection*: five Grenadilla wood beams, with block-rectangular form and dimensions of $260 \times 40 \times 40\ \text{mm}^3$, possessing straight fiber in the longitudinal direction (L) and clearly defined tangential (T) and radial (R) directions, were chosen. These beams came from Tanzania and included only the heartwood part.

(b) *Cutting plan*: for each beam, samples for sorption, diffusion and swelling–shrinkage experiments were produced. Samples were cut according to the schematic shown in Fig. 1. For each direction, 3 thicknesses were used: 3 mm, 6 mm and 12 mm, each sample having a section of dimensions $33 \times 30\ \text{mm}^2$. Each of those samples used for diffusion experiments also had their sides (thickness × width and thickness × length) sealed using aluminum adhesive tape (Fig. 1b), which was chosen on the basis of the total absence of hygroscopicity of its material and on its airtightness to air humidity, following the pretests carried out by packing a metallic plate with it and putting the sample in a controlled climatic chamber. Concerning the swelling–shrinkage and adsorption–desorption experiments, 3 samples were procured from each beam; each of them was cut with the dimension of 30 mm (T or R direction) × 35 mm (R or T direction) × 6 mm (L direction). More detailed information regarding the dimensions is given in Table 1. In the end, after removing the samples with defects, we had 10 samples for the swelling–shrinkage experiments and 87 for the diffusion experiments, of which 27 (those 3 mm thick) were also used for sorption.

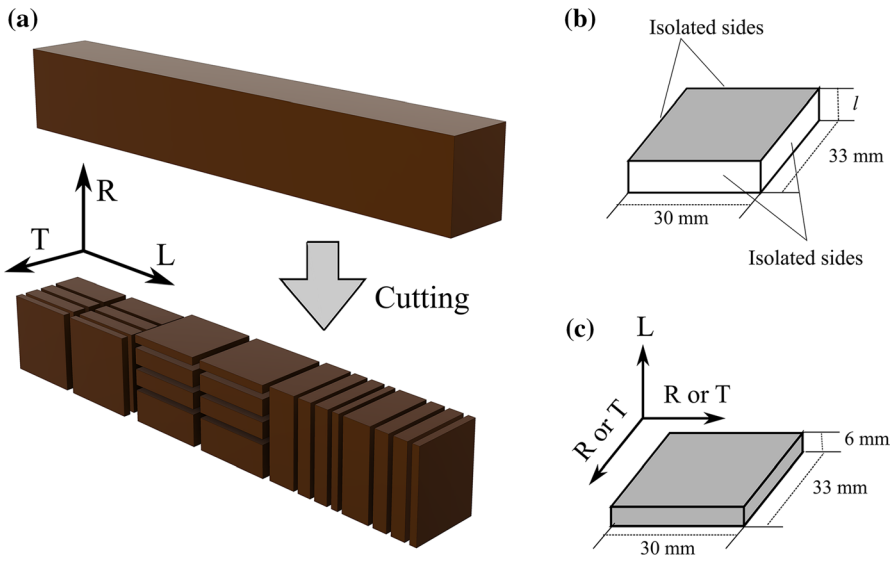

Fig. 1 Sampling plan schematic for hygroscopic characterizations: **a** cutting plan from the rectangular-block beam toward small samples, **b** diffusion/sorption samples, with $l = 3$, 6 or 12 mm and **c** swelling–shrinkage samples

Table 1 Sampling code, dimensions and orientations

Sample type	Code	Thickness (direction)	Width (direction)	Length (direction)
Diffusion/sorption	DT	3 (T)	30 (R or L)	33 (L or R)
Diffusion	DT	6 (T)	30 (R or L)	33 (L or R)
Diffusion	DT	12 (T)	30 (R or L)	33 (L or R)
Diffusion/sorption	DR	3 (R)	30 (L or T)	33 (T or L)
Diffusion	DR	6 (R)	30 (L or T)	33 (T or L)
Diffusion	DR	12 (R)	30 (L or T)	33 (T or L)
Diffusion/sorption	DL	3 (L)	30 (R or T)	33 (T or R)
Diffusion	DL	6 (L)	30 (R or T)	33 (T or R)
Diffusion	DL	12 (L)	30 (R or T)	33 (T or R)
Swelling–shrinkage	S1	6 (L)	30 (T)	33 (R)
Swelling–shrinkage	S2	6 (L)	30 (R)	33 (T)

All values are in mm

Sampling for mechanical characterization

The mechanical characterization in this study was carried out using a nondestructive method based on the measurement of ultrasound wave propagation speed. Taking into account the orthotropical properties of wood, an adapted sampling plan similar to those used in other past studies (Bucur 2006; Gonçalves et al. 2014) was prepared as follows:

(a) *Material selection*: five grenadilla wood specimens, one per beam, were cut into cuboid shape, with the size of $20 \times 20 \times 20\,mm^3$ (L, R and T direction) (Fig. 2a). Only specimens with good fiber orientation and consisting solely of heartwood were chosen.
(b) *Cutting plan*: the specimens were cut using CNC (computer numerical control) machine into a polyhedron (Fig. 2b). The 5 resulting samples were then used for the mechanical characterization.

Hygroscopic characterization

Adsorption–desorption: EMC experiments

Several models have been used successfully to fit sorption isotherms of the gravimetric response of wood to steps of constant relative humidity at a given temperature, such as the HH model (Hailwood and Horrobin 1946) or the Guggenheim, Anderson and de Boer (GAB) equation (Maroulis et al. 1988), including tropical species (Simo-Tagne et al. 2016a, 2019). Here, the sorption model developed by Merakeb et al. (2009) was adopted because of its thermodynamic basis, its limited number of parameters and its applicability to describe total and partial desorption and adsorption curves. In that

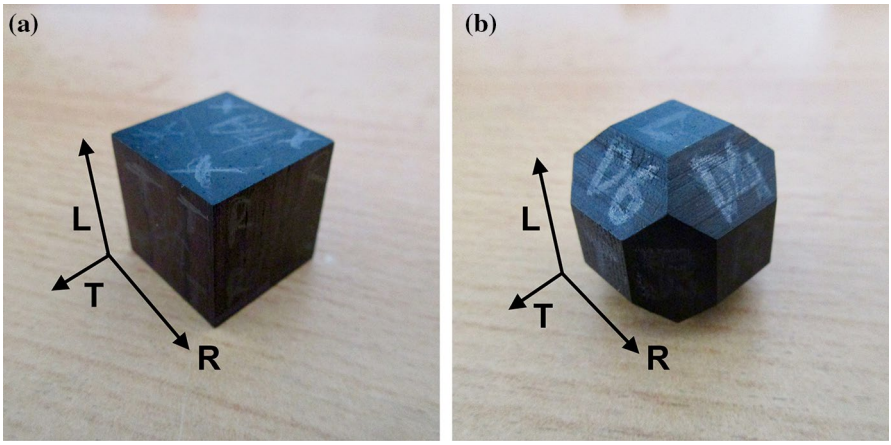

Fig. 2 Sampling plan schematic for mechanical characterizations: **a** original cuboid sample and **b** polyhedron sample cut from the cuboid sample

model, the empirical approach of Pederson (1990) was used to describe partial isotherms, giving the moisture content (MC) at the equilibrium state for successive steps of h and T (Pederson 1990; Rode and Clorius 2004; Carmeliet et al. 2005; Varnier et al. 2020).

For a full-cycle sorption, the formulation of this model can be written as (Merakeb et al. 2009):

$$\ln\left(\frac{W}{W_s}\right) = \phi \times \ln(h) \times \exp(\alpha h), \tag{1}$$

$$W(h,T) = W_s(T) \times \exp\left[\phi \times \ln(h) \times \exp(\alpha h)\right], \tag{2}$$

where $W(h, T)$ refers to the MC as a function of the relative humidity (h) and temperature (T), while $W_s(T)$ refers to the fiber saturation point of wood as a function of T; α and ϕ are thermodynamic parameters determined for both adsorption (α_a and ϕ_a) and desorption (α_d and ϕ_d).

For the partial-cycle curve, an empirical weighing formulation is used (Varnier et al. 2020). The equations can be written as:

$$W_f = W_i + \xi_a \times (h_f - h_i), \tag{3}$$

for adsorption and

$$W_f = W_i + \xi_d \times (h_f - h_i), \tag{4}$$

for desorption. W_i refers to W at initial h_i, while W_f refers to W at final h_f. The weighed parameter (ξ) is described by (Pederson 1990; Kulasinski 2015; Varnier et al. 2020):

$$\xi_a = A \times \zeta_d \left| \frac{W_i - W_a}{W_d - W_a} \right|^{\beta} + \zeta_a \left| \frac{W_d - W_i}{W_d - W_a} \right|^{\beta}, \tag{5}$$

for adsorption and for desorption:

$$\xi_d = \zeta_d \left| \frac{W_i - W_a}{W_d - W_a} \right|^{\beta} + K \times \zeta_a \left| \frac{W_d - W_i}{W_d - W_a} \right|^{\beta}, \tag{6}$$

where W_a and W_d refer to the W values on adsorption and desorption curve (Eqs. 1–2) with $h = h_i$ referred in both Eqs. 3 and 4. Finally, ζ_x is described as (Rode and Clorius 2004; Carmeliet et al. 2005):

$$\zeta_x = \frac{\partial W_x}{\partial h} = W_s \left(\alpha\phi \exp(\alpha h) \ln(h) + \frac{\phi \exp(\alpha h)}{h} \right) \exp(\phi \exp(\alpha h) \ln(h)), \tag{7}$$

with $\alpha = \alpha_a$ and $\phi = \phi_a$ for $\zeta_x = \zeta_a$ or $\alpha = \alpha_d$ and $\phi = \phi_d$ for $\zeta_x = \zeta_d$.

The sorption samples were distributed with 14 in group "cycle A" and 13 in group "cycle B." All samples were put in a climate chamber, type Memmert HPP 110, at $T = 20\,°C$ (ISO standards and mean temperature for the use of this wood in northern countries) and several humidity conditions (consecutively, as detailed in Table 2) with the equilibrium mass (m in gram) of each sample measured at each step. The reason for having two cycles (A and B) instead of only one is that, as we can see in Table 2, cycle A has a smaller isotherm cycle than B. This was useful during the estimation of the isotherm model parameters using curve-fitting method: Instead of only having one partial cycle (from the dry state to close to the saturated one), we have a second smaller partial cycle that allows to identify parameters for limited hygrometric variations in the hygroscopic domain. Thus, the estimation of the isotherm model parameters would be more robust and applicable to any case. The curve-fitting calculations were conducted using MATLAB with Curve Fitting Toolbox® (Mathworks 2018a).

To ensure that the final mass is as close as possible to that of the equilibrium level, we proceed to the next step only when the masses of the samples do not change more

Table 2 Humidity steps of EMC experiments at $T = 20\,°C$ where h is the relative humidity of the climate chamber (fractional)

Steps no.	Cycle A		Cycle B	
	h	Note	h	Note
1	0.85	First stabilization	0.65	First stabilization
2	0.65	Desorption	0.85	Adsorption
3	0.45	Desorption	0.65	Desorption
4	0.25	Desorption	0.45	Desorption
5	0.00	Drying	0.25	Desorption
6	0.25	Adsorption	0.45	Adsorption
7	0.45	Adsorption	0.65	Adsorption
8	0.65	Adsorption	0.00	Drying
9	0.00	Drying	–	–

than 0.001 g (variation ≈0.03% of the sample's initial mass, smaller than the 0.1% per day usually required in the standards) between measurements, which were, on average, conducted once a day. The stabilization time for one step was around 2 to 3 days, as will be shown in the Results section. The measurements were taken using a Mettler Toledo ME204 scale, with a displayed precision of 0.0001 g.

The final step is drying the samples completely using vacuum-drying method, deployed together with P_2O_5 for absorbing the evaporating moisture at $T = 60\,°C$, so that the moisture content for each h level can be derived. Drying at a reduced temperature is necessary to prevent the extractives from leaking out of the sample.

Diffusion experiments

The diffusion experiments were performed with several h steps inside a climate-controlled chamber, just like the adsorption–desorption experiments. The relative humidity conditions are detailed in Table 3.

The mass of each sample, including the aluminum adhesive tape, was measured periodically (on average, once every three hours for the first day of stabilization at a new level of h, followed by twice a day afterward). Every time all of the samples reached their equilibrium state, which means their mass changes fall within the value of only ±0.001 g between measurements (similar to the method for equilibrium moisture content, "Adsorption–desorption: EMC experiments" section), we moved to the next step to do the diffusion processes again with the mass measurements conducted periodically until the samples reached their equilibrium state. This continued until the 4th step, after which the whole samples were collected and dried completely so that their moisture content (W) can be calculated. Note that it is assumed that the mass of the aluminum adhesive tape does not change with the relative humidity, as it was shown during the pretest carried out by packing a metallic plate with it.

By assuming zero free water inside the wood samples (as is the case for $W < W_s$), the concentration of moving bound water during the diffusion process can be written as:

$$\frac{\partial c}{\partial t} = \nabla \cdot (D \nabla c), \tag{8}$$

where c is the diffusing concentration of moisture, t the diffusion time and D the coefficient of diffusion (Crank 1979). In the case of wood, as an orthotropic material,

Table 3 Steps of diffusion experiments where h is the relative humidity of the climate chamber (fractional)

Steps no.	Step type	T(°C)	h
1	First stabilization	20	0.30
2	Adsorption	20	0.50
3	Adsorption	20	0.70
4	Adsorption	20	0.90
5	Complete drying in vacuum dryer $+P_2O_5$	60	0.0

D can be expressed as a tensor of three diffusion coefficients (D_L, D_R and D_T for diffusion in L, R and T direction, respectively) and its matrix written as follows (Eitelberger and Hofstetter 2010) in the main direction of orthotropy:

$$[D] = \begin{bmatrix} D_L & 0 & 0 \\ 0 & D_R & 0 \\ 0 & 0 & D_T \end{bmatrix}. \tag{9}$$

To determine these diffusion coefficients, we adapted the experimental method conducted in previous studies (Olek and Weres 2007). As detailed in "Sampling plan" section, before diffusion, samples with three different thicknesses and sealed sides were prepared (Fig. 1a, Table 1) so that only unidimensional diffusion can occur on the desired direction.

Next, we solved the diffusion equation itself by two methods: analytical and numerical.

Analytical method For the analytical method, by assuming a constant coefficient of diffusion D_0, the analytical solution can be written as (Crank 1979):

$$\frac{c(x,t) - c_i}{c_f - c_i} = 1 - \frac{4}{\pi} \sum_{n=0}^{\infty} \exp(-\frac{D_0(2n+1)^2\pi^2 t}{4X^2}) \cos(\frac{(2n+1)\pi x}{2X}), \tag{10}$$

where c_i and c_f refer to the initial and final diffusing concentration, while X refers to the half-thickness of the sample, x refers to the coordinate in thickness from the middle of the sample of a point inside the sample and $c(x, t)$ refers to the concentration at point x at time t.

Derived from the above solution, the ratio between the total change of moisture content at a given time t (M_t) and the total final change in moisture (M_f) can be written as (Crank 1979):

$$\frac{M_t}{M_f} = 1 - \sum_{n=0}^{\infty} \frac{8}{(2n+1)^2\pi^2} \exp(-\frac{D_0(2n+1)^2\pi^2 t}{4X^2}). \tag{11}$$

Experimentally, this ratio of M_t/M_f can be measured as (Siau 1984):

$$\frac{M_t}{M_f} = \frac{W_t - W_i}{W_f - W_i}, \tag{12}$$

where W_t refers to W measured at time t, while W_i and W_f are initial and final W, respectively. As the sum is infinite in Eq. 11, it is usual to compute an approximate value for a finite number of n. Thus, Siau (1984) simplified this equation as follows:

$$\frac{M_t}{M_f} = 1.0 - 0.811 \exp(-2.47 \frac{tD}{X^2}), \tag{13}$$

for $tD/X^2 > 0.2$, where only the first exponential term ($n = 0$) is necessary, and

$$\frac{M_t}{M_f} = 1.13\sqrt{\frac{tD}{X^2}}, \tag{14}$$

for $tD/X^2 < 0.2$. This last equation is an adjustment by a square root function of Eq. 11 for n varying from 0 to several tens. Together, Eqs. 13 and 14 were combined here for estimating the coefficient of diffusion in its constant form (D_0).

Numerical method For the numerical method, the diffusion equation (Eq. 8) was solved using finite element method (FEM) using MATLAB Partial Differential Equation Toolbox® (Mathworks 2018b). In this method, two kinds of approach were used: The first is by assuming that the coefficient of diffusion is a linear function of W, while the second is by assuming that it varies exponentially with W (Olek and Weres 2007). These approaches can be expressed as follows:

$$D_{lin} = p \cdot W + b, \tag{15}$$

$$D_e = D_0 \cdot \exp(k \cdot W), \tag{16}$$

where p, b and k are empirical constants whose values have to be estimated and D_0 is the value obtained through Eqs. 13 and 14 (analytical model).

Fitting the models to the experimental results The coefficient of diffusion was estimated using optimization method by fitting the analytical and numerical curves to the experimental, measured, data using least-squares method in MATLAB Curve Fitting Toolbox® (Mathworks 2018a), similar to what was used for estimating the sorption isotherm parameters. To evaluate the quality of the fitting, a goodness-of-fit parameter *sse* or sum of squares due to error was used. This statistical parameter measures the sum of deviation of the values generated by the fitted model to the data.

Swelling–shrinkage measurements

The measurements of swelling–shrinkage, or the hygroelastic expansion caused by the changes in W, were taken using the adsorption–desorption samples with the same experimental steps as the EMC experiments (Table 2). The relationships between the dimensional variations and W can be written as:

$$\epsilon = \gamma \times \left(W_f - W_i\right), \tag{17}$$

where W_f and W_i are the W at h_f and h_i, respectively (referred to in Eqs. 3 and 4), γ refers to the swelling–shrinkage coefficient (to be measured) and ϵ refers to the longitudinal strain caused by changes in W, calculated by the following equation in a given main direction:

$$\epsilon = \left(Y_f - Y_i\right)/Y_i, \tag{18}$$

where Y_f and Y_i refer to the final and initial dimensions measured during the final stable condition ($W = W_f$) and the initial condition ($W = W_i$), respectively.

Each swelling–shrinkage coefficient was determined through fitting the experimentally measured strain (Eq. 18) to the mathematical model (Eq. 17). Due to the limited amount of material available, the sample size in the L direction is too small to measure the strain in that direction, and so, we were not able to measure γ_{L}. Finally, to better compare the present results to past studies, the DIN 52184 standard was used to calculate the rate of volume swelling as the total of swelling rate in the radial, tangential and longitudinal directions, written as:

$$\Gamma_v \approx \Gamma_{\mathrm{R}} + \Gamma_{\mathrm{T}} + \Gamma_{\mathrm{L}}, \tag{19}$$

where

$$\Gamma_x(W) = \left(Y_w - Y_0\right)/Y_0, \tag{20}$$

in which $\Gamma_x(W)$ is the swelling rate in a given direction (x = T, R or L) during a particular level of moisture content (W), Y_W is the wood dimension in a certain direction on a particular W level of moisture content, while Y_0 is the dimension of wood in the said direction under complete anhydrous condition. In this way, this makes Γ to be equal to ϵ if Y_f is equal to Y_W and Y_i to Y_0. As we were not able to measure Γ_{L}, and as $\Gamma_{\mathrm{L}} \ll \Gamma_{\mathrm{R}}$ or Γ_{T}, $\Gamma_v \approx \Gamma_{\mathrm{R}} + \Gamma_{\mathrm{T}}$.

Mechanical properties

The mechanical characterizations were conducted using ultrasound method. Particularly, the properties here were those of the stiffness matrix $[C]$. By determining $[C]$, we could then determine the compliance matrix $[S] = [C]^{-1}$. We did this by linking the phase velocity of the ultrasound wave to the stiffness parameters. The solutions of these equations were used to develop the ultrasonic method for determining the elastic constants of anisotropic materials (Bucur and Archer 1984; François et al. 1998; Gonçalves et al. 2014; Bachtiar et al. 2017).

Bachtiar et al. (2017) used different cubic samples with different orientations and did an in-depth analysis of the associated equations between the wave velocity and the elastic parameters C_{ii}. For the present study, the method developed by Gonçalves et al. (2014) was adapted, which uses polyhedron samples (Fig. 2b), because of its practicality and capability to measure all the elastic parameters using only one sample.

Experimental protocol

Determining the density The density of the five samples used for the ultrasonic measurements was obtained by using gravimetric methods ($\rho = m/\mathrm{V}$). The mass (m) of the sample was measured using a Mettler Toledo ME204 scale, which was also used for the EMC and diffusion experiments ("Adsorption–desorption: EMC experiments" and "Diffusion experiments"). The volume (V) was measured using Mitutoyo digital caliper with a displayed precision of 0.01 mm when the specimens were in

their cuboid form (Fig. 2) with 2 measurements for each direction. The mass and volume of the samples were determined at $h = 0.45$ and $T = 20°C$, as for all ultrasonic measurements.

Ultrasonic measurements The tools used in the ultrasonic measurements consist of an ultrasonic generator Sofranel PR5072, oscilloscope Tektronik TDS3032 with N acquisitions of 10,000 points with $f = 500$ MHz at 9 bits, and Sonaxis longitudinal (CMP 123) and transverse (CMP 124) probes with active diameter of 15 mm and central frequency of 500 kHz.

The measurements were taken in transmission. First, a reference echo was recorded by placing both probes in contact. Then, the experimental echo was recorded by placing both probes on the surfaces of the specimens facing each other, so that the echo passes through the sample from one probe and is captured by the other.

The transmitting probe was excited with a wave train (tone burst) of 5 cycles at 500 kHz and amplitude 10 Vpp (maximum voltage of the generator). The choice of these parameters has been made through previous tests and literature review. To ensure a good transmission through wood specimens, the frequency was chosen lower than those usually used for such testing to reduce damping. However, below 500 kHz, most ultrasonic probes have small frequency bandwidth. Therefore, duration of echoes is too large, they overlap and precise measurement of the speed of sound is not possible. The bandwidth of the burst was narrow enough to obtain an almost monochromatic transmitted signal. Under these conditions, the group velocity differed very little from the phase velocity (Brillouin 2013; Orfanidis 2016). The time of flight was then deducted by calculating, using MATLAB's Signal Processing Toolbox (Mathworks 2018c), the maximum of the envelope of the inter-correlation between the reference echo and the ones that passed through the sample.

In addition, the wavelength was small enough to measure the velocities of a semi-infinite medium (Tu et al. 1955; Ashman et al. 1984), which made it possible to determine the stiffness matrix according to the propagation direction and polarization of the wave. The acoustic coupling was achieved using honey. It is a coupling medium that has been shown to be effective for shear waves and has been widely used in previous studies using ultrasound testing on materials (Kohlhauser et al. 2009; Camara et al. 2010; Cegla et al. 2011). In addition, it is very easy to remove with a minimum of water and penetrates very little into samples, so it does not induce significant variation in mass or moisture.

Determining the stiffness matrix components

The diagonal components of the $[C]$ matrix (C_{ii}, where $i = 1, 2, 3, \ldots 6$) were determined using the measurement of three longitudinal and three shear wave velocities propagating along the principal axes (L, R and T) and the density of the sample (Table 4).

Afterward, using the phase velocities measured at an angle θ from the main axis (V_θ) and the corresponding stiffness components, and by considering that the matrix

[C] is a symmetrical one, the remaining three components (C_{12}, C_{13} and C_{23}) were calculated using the methods described by Bachtiar et al. (2017). Note that the computation of the elastic constants was performed for each sample using its own data before averaging.

Results

Wood density

Firstly, it was found that the density of this wood, measured at $T = 20\,°C$ and $h = 0.45$, is equal to $1250.0 \pm 26.2\,kg/m^3$. This value is comparable to other studies, which were in the range of 1100 to 1400 kg/m^3 (Zadro 1975; Gérard et al. 2017; Sproßmann et al. 2017; Liu et al. 2020). Such value confirms grenadilla's position as a commercial wood with one of the highest densities in the market.

Adsorption–desorption (EMC) curves

The mean (μ) and standard deviation (δ) values of the sorption parameters, identified by fitting the curves of the models (Eqs. 1–7) on the experimental data from the samples of cycles A and B simultaneously, were successfully estimated (Table 5). The experimental data and the sorption model were also plotted together on the adsorption–desorption graph (Fig. 3). Note that only one set of parameters (Table 5) for all cycles was used.

Several points could be noted. Firstly, during the experiments, before the first stabilization of cycle A and cycle B samples (Table 2), all the specimens have been kept at room condition ($T \approx 20\circ$ C and $h \approx 0.45$). Therefore, it came as no surprise to us when we saw that all samples, during their first stabilization, experienced *adsorption* (not shown here). This is a small detail, but it should be noted for any experiments aiming to determine the adsorption–desorption parameters of wood. Moreover, Fig. 3 shows that the starting point of cycle A is outside the complete cycle. It is assumed that this is due to the fact that the equilibrium was not reached

Table 4 Determining the diagonal components of the stiffness tensor (C_{ii})

Component	Wave type	Direction of propagation	Direction of polarization	Formula
C_{11}	Longitudinal	L (1)	–	ρV^2_{LL}
C_{22}	Longitudinal	R (2)	–	ρV^2_{RR}
C_{33}	Longitudinal	T (3)	–	ρV^2_{TT}
C_{44}	Shear	R (2) or T (3)	T (3) or R (2)	ρV^2_{RT} or ρV^2_{TR}
C_{55}	Shear	L (1) or T (3)	T (3) or L (1)	ρV^2_{LT} or ρV^2_{TL}
C_{66}	Shear	L (1) or R (2)	R (2) or L (1)	ρV^2_{LR} or ρV^2_{RL}

Table 5 Identified material parameters (unitless) of the sorption model (Eqs. 1–7)

Parameters	W_s	ϕ_a	ϕ_d	α_a	α_d	A	β	K
μ	0.173	1.226	0.517	0.620	0.657	0.158	0.265	0.024
δ	±0.003	±0.109	±0.018	±0.196	±0.268	±0.135	±0.087	±0.041

for the first step of this cycle, when we have moved on to the next step. This starting point was thus considered as non-reliable and not taken into account during the curve-fitting.

Next, we saw that the identified model, calculated using the mean values of the sorption parameters (Table 5), produces partial-cycle curves that fit quite well to the experimental data. Furthermore, the full-cycle model, here visualized in Fig. 3 using discontinuous black line, also contains all the experimental data and partial model. This shows that the obtained parameters here are well adapted for grenadilla wood.

However, several cautions should be known. Firstly, it should be noted here that the parameters were estimated at a temperature of 20 °C. Other temperatures could produce different material properties, especially for the fiber saturation point (W_s), which has been known to vary with the temperature T (Berry and Roderick 2005; Zelinka et al. 2016; Varnier et al. 2020). Still regarding the fiber saturation point obtained here ($W_s = 0.173(3)$, Table 5), it was estimated through the curve-fitting instead of an experimental method, such as those conducted by Simpson (2001), because we do not possess grenadilla wood specimen in its green or freshly cut condition. The efforts to return wood to its green state by soaking it in the water until its moisture content reaches more than 0.30—where $W = 0.30$ is the mean fiber saturation point for many wood species (Glass and Zelinka 2010; Berry and Roderick 2005; Simpson 2001)—failed because, during the soaking process, part of the extractives of these samples came out and solubilized in water, thus making its

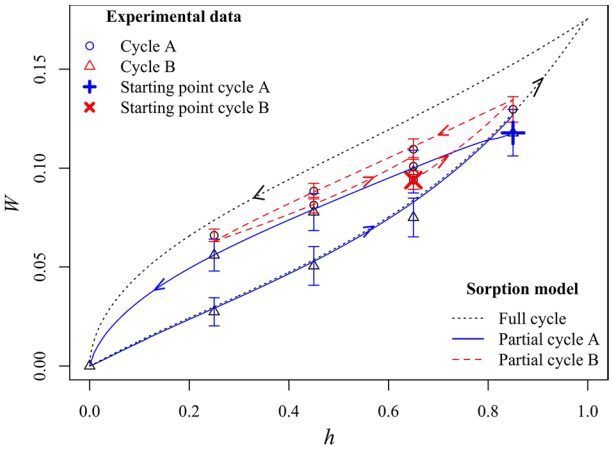

Fig. 3 Experimental data and curves of the full and partial cycles of the identified adsorption–desorption model: arrows going up indicate adsorption, while arrows going down indicate desorption

final native "green" state highly questionable. Thus, future efforts in determining the "true" W_s of grenadilla, by drying samples from their green state and determining the moisture content when they start to shrink, should be made by firstly obtaining wood samples in its green state.

Nevertheless, the value of W_s found here is comparable to those found by Gérard et al. (2017) (0.25) and Liu et al. (2020) (0.11). In regard to the low value of W_s that was found for grenadilla wood, one of the factors that could play an important role here is the presence of extractives. Past studies have shown that the extractives could significantly affect the hygroscopic properties of wood, particularly in preventing the bonding of water molecules with the wood cell walls (Choong 1969; Chen and Choong 1994; Nzokou and Kamdem 2004). Another, less important, factor could be the cellulose crystallinity. As described by Fernández et al. (2014), who conducted a study comparing the sorption and thermodynamic properties of obeche and limba wood—two species from Africa—a higher crystallinity index could lead to a lower proportion of amorphous part in cellulose, which implies less bonds with water molecules, thus leading to a lower fiber saturation point. To the authors' best knowledge, the crystallinity index of grenadilla has not been measured so far. Thus, this parameter, as well as the extractive content (mainly) and their effects on sorption and the fiber saturation point, could be important to study in the future.

Diffusion coefficients

The diffusion coefficient was determined for the three directions L, R and T using both the analytical (constant coefficient) and numerical solutions (non-constant coefficient), together with the local relative errors for all methods. The results are given in Table 6, where the values for D are given in cm^2/s. The difference between the diffusion in L, R and T directions is visible in Fig. 4: L diffusion is the fastest one, while R is slightly quicker than T, although not very significantly, particularly at high-humidity condition.

Among the three approaches used to estimate the diffusion coefficients, the linear model given by Eq. 15 produced the smallest error values *sse* for all three directions although the difference between the *sse* values for each model in each direction is not significant. It should be noted that this phenomenon could be marked as normal because the variation of the non-constant diffusion coefficient with the moisture contents itself is small, only 10–20% maximum for W varying from 0 to 0.15.

Moreover, among the three directions, the *sse* values for the diffusion in L direction were the lowest. This indicates that the results of our curve-fitting model is better for D_{L} than for D_{R} or D_{T}. Moreover, if the present coefficient of variation (CV) of the coefficients of diffusion was calculated as the ratio between their standard deviation δ and the mean value μ (thus $\mathrm{CV} = \mu/\delta$, data from Table 6), we can see that the CV of $D_{0_{\mathrm{L}}}$ (18.34%) is lower than those of $D_{0_{\mathrm{R}}}$ (35.78%) and $D_{0_{\mathrm{T}}}$ (31.82%). This could be due to the fact that, as shown in Fig. 4, samples in the R and T directions, contrary to the L direction, have not exactly reached the equilibrium before the change to the next step in relative humidity, and therefore, diffusion is almost always in an unstable or transient state, and moisture content inside the sample is

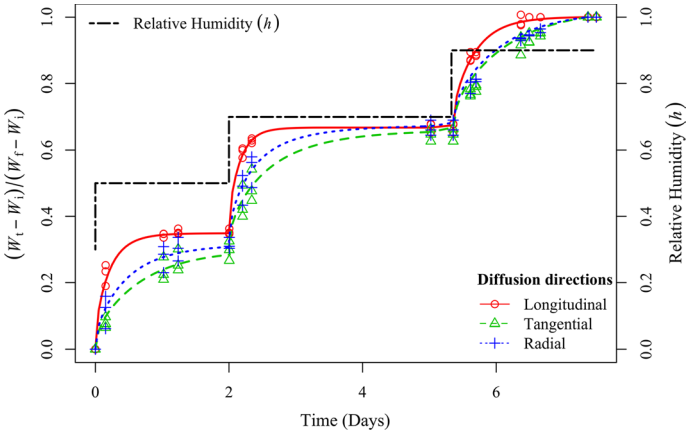

Fig. 4 Experimental data (points) compared to the analytical model (lines) for a constant diffusion coefficient for samples with a thickness of $l = 3$ mm

not completely homogeneous. This is not a problem with the numerical approach, where the adjustment was made for each curve in its entirety with all the h steps. In this case, the diffusion profile along the thickness of the sample is calculated and then integrated to obtain the variation in mass of the sample, so that it can take into account a non-homogeneous initial state when the relative humidity condition changes. However, it is true that this poses a problem for the analytical approach (for constant diffusion coefficient) because Eqs. 13 and 14 assume a homogeneous initial state of the sample. Nevertheless, computation of the moisture content profile at the end of a h step shows that this deviation from homogeneity seems negligible compared to the measurement variability. Another possible explanation for the better adjustment in the L direction is that the anatomical variation along the L direction is lower than those in the R and T directions, who are subjected more to irregularity caused by the varying cell distribution and density during cambial growth (Tateishi et al. 2008; Nugroho et al. 2012; Tanabe et al. 2018).

The relationship between wood density and diffusion coefficient can be discussed as well. Past studies have shown the link between these two parameters. In particular, Siau (1984) has formulated the relationships in terms of not only density but also porosity and cell distribution. Compared to the coefficients of diffusion of other wood species found in other studies (Table 7), and by reporting them in a graph (Fig. 5), several important points could be noted.

Firstly, the relationships between the wood density and coefficient of diffusion could be clearly seen with a simple power function. We saw that, aside from the fitted line for D_L, the other coefficients of diffusion seem to correspond well with their model. Not only that, the coefficients of diffusion for the tangential direction also fit to the modelized D_T curve calculated by Siau (1984). Moreover, the values of D_0 for grenadilla (constant value, Eq. 11) match quite well to these fitted lines, except for D_L which seems to be significantly lower than both the fitted lines calculated from the data of other studies and the model of Siau (1984).

This shows the possibility of other factors in play for the diffusion in L direction, such as the presence of extractives, which has been known to be very abundant in *Dalbergia* wood, with a strong presence in lumens (Donnelly et al. 1975; Gérard et al. 2017; Yin et al. 2018), and their role in moisture transfer in wood has been shown, mostly because of their water solubility properties (Choong 1969; Chen and Choong 1994). Furthermore, it has been found that extractives lower the dynamic sorption process and hygroscopicity of wood (Yang et al. 2018).

Swelling–shrinkage

The strain evolution was correlated with the moisture content variation, and the swelling–shrinkage coefficients were thus determined (Fig. 6). Swelling–shrinkage coefficients equal to 0.32 ± 0.05 in T direction (γ_T) and 0.20 ± 0.03 in R direction (γ_R) were obtained. In L direction, unfortunately, the dimensional changes were too small to be accurately measured. Efforts in future studies should be directed toward determining a feasible method to measure it with a limited amount of wood.

To compare the present results to a previous study, which also implemented the calculation method in accordance with the DIN 52184 standard (Eqs. 19 and 20), we have calculated the volumetric swelling coefficient Γ_V from an oven-dry initial condition toward $h = 0.85$. We took the adsorption–desorption parameters obtained (Table 5) and calculated the final moisture content (W_f) value as 0.122. Thus, obtaining $\Gamma_R(W = 0.122) = 0.024$ and $\Gamma_T(W = 0.122) = 0.038$, we found $\Gamma_V = 0.062$ for this condition. This value is still within the range of the Γ_V found by the previous study, which is $5.17 \pm 1.44\%$ (Sproßmann et al. 2017). Moreover, Liu et al. (2020) have measured the swelling rate in the R and T directions (Eq. 20) following the ISO 13061-15 and ISO 13061-16 standards and they obtained $\Gamma_R = 0.028$, $\Gamma_T = 0.032$ and $\Gamma_V = 0.064$, for a density of 1360(100) kg/m^3, very close to the values obtained

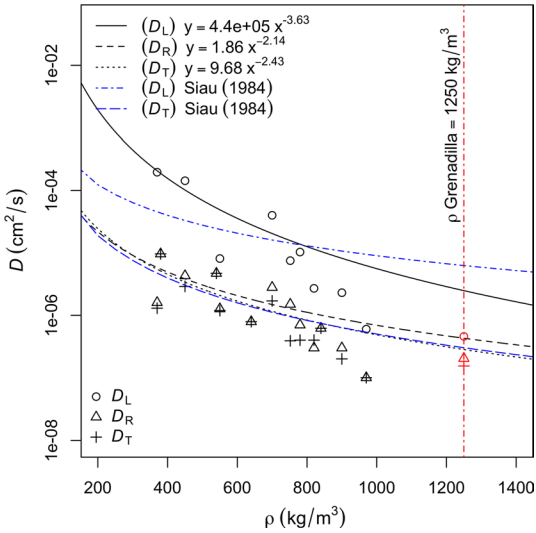

Fig. 5 Relationships between the diffusion coefficient and wood density; data taken from published studies and the average values of the grenadilla wood from the present study

Table 6 Parameters and (mean) coefficients of diffusion determined using the three models, constant (D_0, Eq. 11), linear (p, b, D_{lin}, Eq. 15) and exponential (k, D_e, Eq. 16) and their respective errors

Direction	$D_0(\times 10^{-7}\ \text{cm}^2/\text{s})$	$p(\times 10^{-7}\ \text{cm}^2/\text{s})$	$b(\times 10^{-7}\ \text{cm}^2/\text{s})$	$D_{\text{lin}}(\times 10^{-7}\ \text{cm}^2/\text{s})$	k	$D_e(\times 10^{-7}\ \text{cm}^2/\text{s})$	sse ($\times 10^{-6}$)
R	2.04 ± 0.73	–	–	–	–	–	1.26 ± 1.00
	–	2.21 ± 0.12	1.91 ± 0.76	2.08	–	–	1.20 ± 1.03
	2.04	–	–	–	0.40 ± 0.26	2.11	1.21 ± 1.03
T	1.54 ± 0.49	–	–	–	–	–	1.77 ± 0.91
	–	2.30 ± 0.22	1.35 ± 0.52	1.54	–	–	1.74 ± 0.91
	1.54	–	–	–	0.28 ± 0.09	1.57	1.76 ± 0.91
L	4.58 ± 0.84	–	–	–	–	–	0.63 ± 0.34
	–	2.28 ± 0.10	4.62 ± 1.06	4.79	–	–	0.51 ± 0.30
	4.58	–	–	–	0.74 ± 0.42	4.86	0.51 ± 0.29

Table 7 Published diffusion coefficients of various wood species and their density used in Fig. 5

Wood species	ρ(kg/cm^3)	D_L($\times 10^{-7}$)(cm^2/s)	D_R($\times 10^{-7}$)(cm^2/s)	D_T($\times 10^{-7}$)(cm^2/s)	Source
Corymbia maculata	970	6.00	1.00	1.00	Redman et al. (2012)
Eucalyptus pilularis	900	23.00	3.00	2.00	Redman et al. (2012)
Eucalyptus marginata	820	27.00	3.00	4.00	Redman et al. (2012)
Eucalyptus obliqua	780	103.00	7.00	4.00	Redman et al. (2012)
Pinus pinaster	450	1430.00	43.00	29.00	Agoua and Perre (2010)
Picea abies	370	1960.00	16.00	13.00	Agoua and Perre (2010)
Fagus sylvatica	752	75.00	15.00	3.90	Olek et al. (2005)
Pinus sylvestris	550	81.10	12.70	11.90	Olek et al. (2005)
Tectona grandis	700	400.00	28.00	17.00	Agoua and Perre (2010)
E. cylindricum	640	–	7.90	7.90	Simo-Tagne et al. (2016b)
Sterculia rhinopetala	840	–	6.20	6.20	Simo-Tagne et al. (2016b)
Triplochiton spp.	380	–	96.30	96.30	Simo-Tagne et al. (2016b)
Terminalia superba	540	–	47.00	47.00	Simo-Tagne et al. (2016b)
Dalbergia melanoxylon	1250.0 ± 26.2	4.58 ± 0.84	2.04 ± 0.73	1.54 ± 0.49	Present study

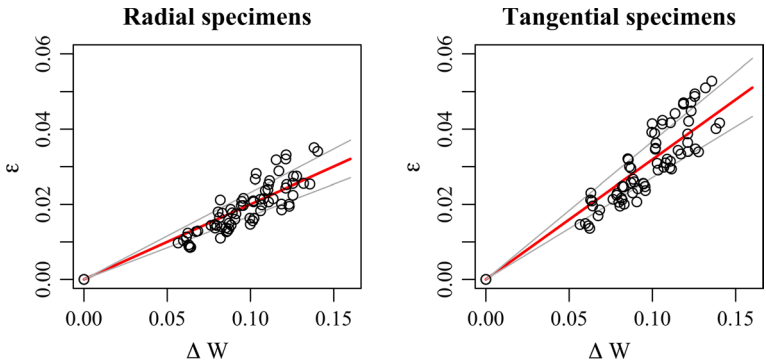

Fig. 6 Evolution of strains caused by the changes in moisture content. Points refer to experimental data, bold lines in the middle to model and the thin lines to standard deviation

here. Finally, the total shrinkage in the R and T directions reported in Gérard et al. (2017), $\Gamma_R(W_S) = 0.029$ and $\Gamma_T(W_s) = 0.048$, agree with the present values too as $\Gamma_R(W_s) = \gamma_R W_s = 0.035$ and $\Gamma_T(W_s) = \gamma_T W_s = 0.055$.

Mechanical properties

Stiffness matrix

According to the designation made for the wave propagation directions (L = 1, R = 2, T = 3, 4 = RT, 5 = LT, 6 = LR), theoretically, the expected values of the matrix components are $C_{11} > C_{22} > C_{33}$ for the longitudinal wave type, $C_{44} < C_{55} < C_{66}$ for the shear wave type and $C_{12} > C_{13} > C_{23}$ for the non-diagonal terms. The measured values fulfilled these conditions (Table 8).

For each sample, the compliance matrix [S] was determined by inverting the stiffness matrix [C] obtained through velocity measurements, and so, the Young's and shear moduli of each sample were obtained. Then, the Poisson's ratios (ν_{ij}) were determined from the non-diagonal components of the [S] matrix. Note that they are usually defined as the negative ratio of the transverse (passive) strain ϵ_{jj} divided by the axial (active) strain ϵ_{ii} during a tensile test in the axial direction i.

Comparison with past studies

The limited amount of literature studying the whole Young's and shear moduli of grenadilla wood makes it a challenge for us to compare the present results to past studies, especially for moduli in R and T directions and shear moduli. Nevertheless, a few publications allowed some comparison.

For the Young's modulus in the L direction (E_L), first the present results were compared to the values obtained by Guitard and El Amri (1987)'s empirical model for $\rho = 1250\,\text{kg/m}^3$ (Tables 9 and 10). As we can see, the mean value of E_L is much lower than theirs. Although a critical point should be stated here, which is the fact

Table 8 Stiffness matrix components (C_{ij}) in GPa with L = 1, R = 2, T = 3, 4 = RT, 5 = LT, 6 = LR

Terms	C_{11}	C_{22}	C_{33}	C_{44}	C_{55}	C_{66}	C_{12}	C_{13}	C_{23}
μ	21.92	7.51	6.16	1.80	2.65	3.17	5.74	5.57	3.42
$\pm\delta$	±3.63	±0.39	±0.31	±0.04	±0.15	±0.22	±0.98	±1.13	±0.27

that Guitard and El Amri (1987) only used four values of data for wood with the density above 900 kg/m^3—thus lowering their applicability to our wood—and their empirical model only gives an order of magnitude of the expected values as they only take the density into account and no other factors such as the microfibril angle or the cell wall chemistry. However, other studies based on quasi-static bending of grenadilla wood samples have also found E_L higher than ours. Sproßmann et al. (2017), for example, measured $E_L = 17.4(24)$ Gpa for a density of 1270(400) kg/m^3. Gérard et al. (2017) found E_L values to be 20.25 Gpa for $\rho = 1290$ kg/m^3, while Chudnoff (1984) obtained 2.98×10^6 Psi ($\approx$ 20.55 GPa) for $\rho = 1080$ kg/m^3 and Liu et al. (2020) 17.9(10) GPa for a density of 1360(100) kg/m^3. Although one study by Obataya and Yamauchi (2012), where they measured the natural frequency in bending and torsion of a beam, has found a value similar to ours (15.90 GPa for E_L with $\rho = 1282$ kg/m^3, measured at $W = 0.062$, $h = 0.60$, $T = 25$ °C), and even though the values from those other studies are clearly much closer to ours than to those of Guitard and El Amri (1987), the fact still remains that our E_L values tend to fall on the lower part of their range.

There are several possible explanations for this. The first is that the present wood samples could perhaps possess angled grain despite efforts to choose and use only samples having the appearance of straight grains and orientations. Other than that, it is also possible that the present wood possesses a high microfibril angle (MFA), which has been known to decrease the elastic modulus of wood in the L direction and to increase the elastic moduli in the transverse directions (Cave and Walker 1994; Astley et al. 1998; Hein et al. 2013). Another possibility is that the grenadilla

Table 9 Young's (E_i) and shear (G_{ij}) moduli in GPa, compared to the empirical model of Guitard and El Amri (1987)

Moduli	E_L	E_R	E_T	G_{LR}	G_{LT}	G_{RT}
μ	15.56	5.10	4.05	3.19	2.62	1.77
$\pm\delta$	±1.79	±0.46	±0.35	±0.21	±0.19	±0.02
Guitard and El Amri (1987)	28.2	4.23	3.21	2.66	2.21	1.14

Table 10 Poisson's ratios (ν_{ij}), compared to the empirical model of Guitard and El Amri (1987)

Ratios	ν_{LR}	ν_{LT}	ν_{RL}	ν_{RT}	ν_{TL}	ν_{TR}
μ	0.41	0.51	0.17	0.42	0.16	0.31
$\pm\delta$	±0.12	±0.13	±0.05	±0.10	±0.02	±0.06
Guitard and El Amri (1987)	0.42	0.44	0.06	0.63	0.05	0.48

could display a *biased* apparent density. The concept of density in solid material is usually defined as the ratio between the mass and volume of the sample. Thus, through simple gravimetric measurement, the density of grenadilla wood is $\rho = 1250.0 \pm 26.2\,\mathrm{kg/m^3}$. However, if we are talking from a mechanical point of view, the only mass that matters is the one coming from the structural part of the wood. In this case, it should be the cell walls. At the same time, grenadilla has been known to possess high level of extractives, which is a non-structural part of the wood but still contribute to its mass (Donnelly et al. 1975; Sjostrom 1993). Yin et al. (2018), specifically, have conducted a thorough study regarding the extractives of grenadilla wood and found that the extractive percentage could reach up to 16.05% from extractions using a mixture of benzene/ethanol alone. This value could be considered high compared to subtropical wood, but in fact quite normal for this tropical wood, which could possess extractive content up to between 20 and 25% (Jankowska et al. 2016), a significant part of which is located in the lumens. This could explain the low value obtained for E_L, because there is a possibility that, if we remove all the extractives, the remaining density of the grenadilla (which would consist solely of the mass of the cells) could be significantly lower than $1250\,\mathrm{kg/m^3}$. Finally, there is the possibility of the presence of defects inside the sample, which unfortunately could not be detected before the experiment without using extensive tomography examinations.

For the shear modulus in LR direction (G_{LR}), we found the range of our result (Table 9) to be higher than that of a previous study (Sproßmann et al. 2017), but our result for G_{LT} is in agreement with the value obtained by Obataya and Yamauchi (2012) of 2.73 GPa. Moreover, the comparison with the predicted value from Guitard and El Amri (1987), in Table 9, shows that the present values are all higher than those predicted. Even if the effect of MFA on shear moduli is not that well documented in the literature, a past study has shown that a higher MFA could apparently lead to higher shear moduli, especially G_{TL}, G_{RL} and also slightly G_{RT} (Bader et al. 2012). Thus, again, the present results, and those of Obataya and Yamauchi (2012), seem to be in agreement with a higher MFA.

Finally, no data exist on the Poisson's ratios and we can only compare them with the rough predictions from Guitard and El Amri (1987) as given in Table 10. It seems that the present results are all in the same order of magnitude. Unfortunately, as said above, the limitations of the empirical model of Guitard and El Amri (1987) and the low number of past studies regarding this wood species limit our ability to make a direct comparison.

Because of those reasons, we believed that future efforts should be directed toward conducting other mechanical characterizations using different methods, either nondestructive using, for example, well-known tools based on free beam vibrations (Brancheriau and Baillères 2002; Brémaud 2012) or on natural frequencies of a cubic sample (Longo et al. 2018) or even classical destructive methods. Further, other factors that affect the mechanical stiffness of wood, such as anatomical features (MFA, rays, etc.) and extractives, must be determined. Thus, future efforts should also be directed toward determining the effects of those other properties on the mechanical characteristics of grenadilla.

Conclusion

The hygromechanical properties of grenadilla, including adsorption–desorption hysteresis model—with its unique set of parameters for both full and partial cycles—diffusion coefficients at $T = 20\,°C$, swelling–shrinkage coefficients and all the elastic moduli, together with all Poisson's ratios, were determined in this study. It was found that grenadilla possesses moisture diffusion coefficients that fit quite well to the relationship model between wood density and coefficient of diffusion of other wood species obtained by past studies. However, the diffusion rate in the longitudinal direction seems to be significantly lower than the extrapolated one based on density, which could be explained by the presence of extractives that dampen the diffusion. Different dependencies of these diffusion coefficients on moisture content were tested, and although the differences were not significant, the best dependence was the linear relationship (where a higher moisture content leads to a higher diffusion coefficient). Furthermore, the swelling–shrinkage coefficients obtained also correspond to other published data on the same wood species. Similar results have been obtained with the mechanical properties for the longitudinal modulus, even if the present result is one of the lowest compared to the literature. Since we measure in addition here all the other elastic constants, all moduli suggest that the tendency would be to have a larger microfibril angle in the present case. Future works should then be directed toward four primary points: (a) comparing the obtained ultrasonic measurements with other nondestructive methods, such as free beam vibration or resonant ultrasound spectroscopy, (b) measuring the anatomical (mainly microfibril angle) and chemical (mainly extractive content and cellulose crystallinity) characteristics of this wood, (c) studying the effect of these characteristics, particularly its extractives, on its hygromechanical properties and (d) using the obtained coefficients of diffusion for predicting the moisture transport phenomena in grenadilla during two- or three-dimensional diffusion.

Acknowledgements This research is a result of cooperation between the Laboratoire de Mécanique et Génie Civil (CNRS, Université de Montpellier), ANRT and Henri SELMER Paris under the working scheme of Ph.D. CIFRE, on which the first author was currently working during the time of the writing of this paper. Special acknowledgments are directed toward Michel Millon and Christophe Gallois from Henri SELMER Paris, Gille Camp from LMGC, Stéphane Fourtier from UMR AMAP CIRAD and Daniel Guibal from UMR BioWooEB CIRAD for their technical support.

Compliance with ethical standards

Conflict of interest The authors declare that they have no conflict of interest during the course of this study.

References

Agoua E, Perre P (2010) Mass transfer in wood: identification of structural parameters from diffusivity and permeability measurements. J Porous Med 13(11):1017–1024. https://doi.org/10.1615/JPorMedia.v13.i11.80

Ashman RB, Cowin SC, Van Buskirk WC, Rice JC (1984) A continuous wave technique for the measurement of the elastic properties of cortical bone. J Biomech 17(5):349–361. https://doi.org/10.1016/0021-9290(84)90029-0

Astley RJ, Stol KA, Harrington JJ (1998) Modelling the elastic properties of softwood. Holz Roh- Werkst 56(1):43–50. https://doi.org/10.1007/s001070050262

Bachtiar EV, Sanabria SJ, Mittig JP, Niemz P (2017) Moisture-dependent elastic characteristics of walnut and cherry wood by means of mechanical and ultrasonic test incorporating three different ultrasound data evaluation techniques. Wood Sci Technol 51(1):47–67. https://doi.org/10.1007/s00226-016-0851-z

Bader TK, Hofstetter K, Eberhardsteiner J, Keunecke D (2012) Microstructure-stiffness relationships of common yew and Norway spruce. Strain 48(4):306–316. https://doi.org/10.1111/j.1475-1305.2011.00824.x

Ball SMJ (2004) Stocks and exploitation of East African blackwood (*Dalbergia melanoxylon*): a flagship species for Tanzania's miombo woodlands? Oryx 38(3):266–272. https://doi.org/10.1017/S0030605304000493

Berry SL, Roderick ML (2005) Plant-water relations and the fibre saturation point. New Phytol 168(1):25–37

Brancheriau L, Baillères H (2002) Natural vibration analysis of clear wooden beams: a theoretical review. Wood Sci Technol 36(4):347–365

Brillouin L (2013) Wave propagation and group velocity. Academic Press, Cambridge

Brémaud I (2012) Acoustical properties of wood in string instruments soundboards and tuned idiophones: biological and cultural diversity. J Acoust Soc Am 131(1):807–818. https://doi.org/10.1121/1.3651233

Bucur V (2006) Acoustics of wood. Springer, Berlin

Bucur V, Archer RR (1984) Elastic constants for wood by an ultrasonic method. Wood Sci Technol 18(4):255–265. https://doi.org/10.1007/BF00353361

Camara VC, Laux D, Arnould O (2010) Enhanced multiple ultrasonic shear reflection method for the determination of high frequency viscoelastic properties. Ultrasonics 50(7):710–715. https://doi.org/10.1016/j.ultras.2010.02.007

Carmeliet J, De Wit M, Janssen H (2005) Hysteresis and moisture buffering of wood. In: Symposium of building physics in the nordic countries, Citeseer, pp 55–62

Cave ID, Walker JCF (1994) Stiffness of wood in fast-grown plantation softwoods: the influence of microfibril angle. For Prod J 44(5):43

Cegla FB, Cawley P, Allin J, Davies J (2011) High-temperature (> 500° C) wall thickness monitoring using dry-coupled ultrasonic waveguide transducers. IEEE Trans Ultrason Ferroelectr Freq Control 58(1):156–167. https://doi.org/10.1109/TUFFC.2011.1782

Chave J, Coomes D, Jansen S, Lewis SL, Swenson NG, Zanne AE (2009) Towards a worldwide wood economics spectrum. Ecol Lett 12(4):351–366. https://doi.org/10.1111/j.1461-0248.2009.01285.x

Chen Y, Choong ET (1994) Determining the effect of extractives on moisture movement using a "continuous" measuring system. Wood Fiber Sci 26(3):390–396

Choong ET (1969) Effect of extractives on shrinkage and other hygroscopic properties of ten southern pine woods. Wood Fiber Sci 1(2):124–133

Chudnoff M (1984) Tropical timbers of the world. U.S. Department of Agriculture, Forest Service, Washington

Crank J (1979) The mathematics of diffusion, 2nd edn. Oxford Science Publications, Oxford University Press, Oxford (oCLC: 554098354)

Détienne P (1990) Les bois exotiques anciens d'ébénisterie et leur identification (Ancient exotic woods of cabinet-making and their identification). BOIS & FORETS DES TROPIQUES 223:69–76

Donnelly DM, O'Reilly J, Whalley WB (1975) Neoflavanoids of Dalbergia melanoxylon. Phytochemistry 14(10):2287–2290

Eitelberger J, Hofstetter K (2010) Multiscale homogenization of wood transport properties: diffusion coefficients for steady-state moisture transport. Wood Mater Sci Eng 5(2):97–103. https://doi.org/10.1080/17480272.2010.489650

Fernández FG, Esteban LG, de Palacios P, Simón C, García-Iruela A, de la Fuente J (2014) Sorption and thermodynamic properties of Terminalia superba Engl. & Diels and Triplochiton scleroxylon K. Schum. through the 15, 35 and 50°C sorption isotherms. Eur J Wood Prod 72(1):99–106. https://doi.org/10.1007/s00107-013-0752-x

François M, Geymonat G, Berthaud Y (1998) Determination of the symmetries of an experimentally determined stiffness tensor: application to acoustic measurements. Int J Solids Struct 35(31):4091–4106. https://doi.org/10.1016/S0020-7683(97)00303-X

Glass SV, Zelinka SL (2010) Moisture relations and physical properties of wood. Wood handbook: wood as an engineering material: chapter 4 Centennial ed General technical report FPL; GTR-190 Madison, WI: US Dept of Agriculture, Forest Service, Forest Products Laboratory, 2010: p 41-419 190:4–1

Gonçalves R, Trinca AJ, Pellis BP (2014) Elastic constants of wood determined by ultrasound using three geometries of specimens. Wood Sci Technol 48(2):269–287. https://doi.org/10.1007/s00226-013-0598-8

Guitard D, El Amri F (1987) Modèles prévisionnels de comportement élastique tridimensionnel pour les bois feuillus et les bois résineux (Predictive models of three-dimensional elastic behaviour for hardwoods and softwoods). Ann For Sci 44(3):335–358. https://doi.org/10.1051/forest:19870305

Gérard J, Guibal D, Paradis S, Cerre JC (2017) Tropical Timber Atlas: Technological characteristics and uses. éditions Quæ, Versailles (oCLC: 1022786485)

Hailwood A, Horrobin S (1946) Absorption of water by polymers: analysis in terms of a simple model. T Faraday Soc 42:B084–B092

Hassold S, Ii PPL, Bauert MR, Razafintsalama A, Ramamonjisoa L, Widmer A (2016) DNA barcoding of malagasy rosewoods: towards a molecular identification of CITES-listed Dalbergia species. PLoS ONE 11(6):e0157881. https://doi.org/10.1371/journal.pone.0157881

Hein PRG, Silva JRM, Brancheriau L (2013) Correlations among microfibril angle, density, modulus of elasticity, modulus of rupture and shrinkage in 6-year-old Eucalyptus urophylla × E. grandis. Maderas Ciencia y tecnología 15(2):171–182. https://doi.org/10.4067/S0718-221X2013005000014

Hillis WE (1971) Distribution, properties and formation of some wood extractives. Wood Sci Technol 5(4):272–289. https://doi.org/10.1007/BF00365060

Innes J (2010) Madagascar rosewood, illegal logging and the tropical timber trade. Madagascar Conserv Dev. https://doi.org/10.4314/mcd.v5i1.57335

IUCN (1998) Dalbergia melanoxylon: World Conservation Monitoring Centre: The IUCN Red List of Threatened Species 1998: e.T32504a9710439. Tech. rep., International Union for Conservation of Nature. https://doi.org/10.2305/IUCN.UK.1998.RLTS.T32504A9710439.en, type: dataset

Jankowska A, Drożdżek M, Sarnowski P, Horodeński J (2016) Effect of extractives on the equilibrium moisture content and shrinkage of selected tropical wood species. BioResources 12(1):597–607. https://doi.org/10.15376/biores.12.1.597-607

Jannot Y, Kanmogne A, Talla A, Monkam L (2006) Experimental determination and modelling of water desorption isotherms of tropical woods: afzelia, ebony, iroko, moabi and obeche. Holz Roh Werkst 64(2):121–124. https://doi.org/10.1007/s00107-005-0051-2

Kohlhauser C, Hellmich C, Vitale-Brovarone C, Boccaccini AR, Rota A, Eberhardsteiner J (2009) Ultrasonic characterisation of porous biomaterials across different frequencies. Strain 45(1):34–44. https://doi.org/10.1111/j.1475-1305.2008.00417.x

Kulasinski K (2015) Physical and mechanical aspects of moisture adsorption in wood biopolymers investigated with atomistic simulations. Ph.D. thesis, ETH Zurich

Lancaster C, Espinoza E (2012) Analysis of select Dalbergia and trade timber using direct analysis in real time and time-of-flight mass spectrometry for CITES enforcement. Rapid Commun Mass Spectrom 26(9):1147–1156. https://doi.org/10.1002/rcm.6215

Liu M, Peng L, Lyu S, Lyu J (2020) Properties of common tropical hardwoods for fretboard of string instruments. J Wood Sci 66(1):1–11

Longo R, Laux D, Pagano S, Delaunay T, Le Clézio E, Arnould O (2018) Elastic characterization of wood by resonant ultrasound spectroscopy (rus): a comprehensive study. Wood Sci Technol 52:383–402. https://doi.org/10.1007/s00226-017-0980-z

Lowe AJ, Dormontt EE, Bowie MJ, Degen B, Gardner S, Thomas D, Clarke C, Rimbawanto A, Wiedenhoeft A, Yin Y, Sasaki N (2016) Opportunities for improved transparency in the timber trade through scientific verification. BioScience 66(11):990–998. https://doi.org/10.1093/biosci/biw129

Malimbwi RE, Luoga EJ, Hofstad O, Mugasha AG, Valen JS (2000) Prevalence and standing volume of *Dalbergia melanoxylon* in coastal and inland sites of southern Tanzania. J Trop For Sci 12(2):336–347

Maroulis Z, Tsami E, Marinos-Kouris D, Saravacos G (1988) Application of the GAB model to the moisture sorption isotherms for dried fruits. J Food Eng 7(1):63–78

Mathworks (2018a) MATLAB and curve fitting toolbox release 2018b. Mathworks, Natick, Massachusetts, USA

Mathworks (2018b) MATLAB and PDE toolbox release 2018b. Mathworks, Natick, Massachusetts, USA

Mathworks (2018c) MATLAB and signal processing toolbox release 2018b. Mathworks, Natick, Massachusetts, USA

Merakeb S, Dubois F, Petit C (2009) Modeling of the sorption hysteresis for wood. Wood Sci Technol 43(7):575. https://doi.org/10.1007/s00226-009-0249-2

Nugroho WD, Marsoem SN, Yasue K, Fujiwara T, Nakajima T, Hayakawa M, Nakaba S, Yamagishi Y, Jin HO, Kubo T, Funada R (2012) Radial variations in the anatomical characteristics and density of the wood of *Acacia mangium* of five different provenances in Indonesia. J Wood Sci 58(3):185–194. https://doi.org/10.1007/s10086-011-1236-4

Nzokou P, Kamdem DP (2004) Influence of wood extractives on moisture sorption and wettability of red oak (*Quercus rubra*), black cherry (*Prunus serotina*), and red pine (*Pinus resinosa*). Wood Fiber Sci 36(4):483–492

Obataya E, Yamauchi H (2012) Applicability of Laminated Veneer Cylinder to Sustainable Production of Woodwind Instruments. Proc 2012 IUFRO (International Union of Forest Reserch Organisation, Copenhagen 2012)

Ogawa S (2018) Impact of imported Chinese furniture on the local furniture sector in Arusha City, Tanzania: focusing on the strategies of furniture-makers for using indigenous timber species. Afr Study monogr Suppl Issue 55:27–47

Olek W, Weres J (2007) Effects of the method of identification of the diffusion coefficient on accuracy of modeling bound water transfer in wood. Transp Porous Media 66(1–2):135–144. https://doi.org/10.1007/s11242-006-9010-6

Olek W, Perré P, Weres J (2005) Inverse analysis of the transient bound water diffusion in wood. Holzforschung. https://doi.org/10.1515/HF.2005.007

Orfanidis S (2016) Electromagnetic waves and antennas, vol 1. Sophocles J. Orfanidis, Hardcover

Parr CS, Wilson N, Leary P, Schulz K, Lans K, Walley L, Hammock J, Goddard A, Rice J, Studer M, Holmes J, Corrigan R Jr (2014) The encyclopedia of life v2: Providing global access to knowledge about life on earth. Biodivers Data J 2:e1079. https://doi.org/10.3897/BDJ.2.e1079

Pederson CR (1990) Combined heat and moisture transfer in building constructions. Ph.D. thesis, Technical University of Denmark

Randriamamonjy TA, Handayani IGAKR, Setyono P (2016) Inefficiency of forestry regulations and management applicability on rosewood (Dalbergia. Spp) exploitation in madagascar: case study of Marojejy and Masoala National Parks. RW J Arts Sci Commer 7(3):41–47. https://doi.org/10.18843/rwjasc/v7i3/05

Redman AL, Bailleres H, Turner I, Perré P (2012) Mass transfer properties (permeability and mass diffusivity) of four australian hardwood species. BioResources 7(3):3410–3424

Remy O (2017) Rosewood democracy. In: Williams A, Le Billon P (eds) Corruption, natural resources and development. Edward Elgar Publishing, Cheltenham, pp 142–153. https://doi.org/10.4337/9781785361203.00019

Rode C, Clorius CO (2004) Modeling of moisture transport in wood with hysteresis and temperature-dependent sorption characteristics. In: Proceedings of the performance of exterior envelopes of whole buildings IX: international conference, 2004, Clearwater, Florida

Rowell RM, Banks WB (1985) Water repellency and dimensional stability of wood. Tech. Rep. FPL-GTR-50, U.S. Department of Agriculture, Forest Service, Forest Products Laboratory, Madison, WI. https://doi.org/10.2737/FPL-GTR-50

Siau JF (1984) Transport processes in wood. Springer, Berlin (oCLC: 840294315)

Simo-Tagne M, Rémond R, Rogaume Y, Zoulalian A, Bonoma B (2016a) Sorption behavior of four tropical woods using a dynamic vapor sorption standard analysis system. Maderas Ciencia y tecnología 18(3):403–412, publisher: Universidad del Bío-Bío

Simo-Tagne M, Rémond R, Rogaume Y, Zoulalian A, Perré P (2016b) Characterization of sorption behavior and mass transfer properties of four central africa tropical woods: Ayous, Sapele, Frake, Lotofa. Maderas, Cienc tecnol 18(1):207–226. https://doi.org/10.4067/S0718-221X2016005000020

Simo-Tagne M, Bennamoun L, Léonard A, Rogaume Y (2019) Determination and modeling of the isotherms of adsorption/desorption and thermodynamic properties of obeche and lotofa using nelson's sorption model. Heat Mass Transf 55(8):2185–2197. https://doi.org/10.1007/s00231-019-02577-2

Simpson WT (2001) Wood: dimensional change from moisture. In: Buschow KHJ, Cahn RW, Flemings MC, Ilschner B, Kramer EJ, Mahajan S, Veyssière P (eds) Encyclopedia of materials: science and technology. Elsevier, Amsterdam, pp 9627–9629. https://doi.org/10.1016/B0-08-043152-6/01743-5

Siriwat P, Nijman V (2018) Online media seizure reports: a tool to monitor CITES implementation in regulating the international rosewood trade. For Pol Econ 97:67–72. https://doi.org/10.1016/j.forpol.2018.09.004

Sjostrom E (1993) Wood chemistry: fundamentals and applications. Gulf Professional Publishing, Houston

Snel FA, Braga JWB, da Silva D, Wiedenhoeft AC, Costa A, Soares R, Coradin VTR, Pastore TCM (2018) Potential field-deployable NIRS identification of seven Dalbergia species listed by CITES. Wood Sci Technol 52(5):1411–1427. https://doi.org/10.1007/s00226-018-1027-9

Sproßmann R, Zauer M, Wagenführ A (2017) Characterization of acoustic and mechanical properties of common tropical woods used in classical guitars. Results Phys 7:1737–1742. https://doi.org/10.1016/j.rinp.2017.05.006

Tanabe J, Ishiguri F, Tamura A, Takashima Y, Ohshima J, Iizuka K, Yokota S (2018) Within-tree radial and among-family variations in wood density, microfibril angle, and mechanical properties in *Picea glehnii*. Silva Fenn. https://doi.org/10.14214/sf.9914

Tateishi M, Kumagai T, Utsumi Y, Umebayashi T, Shiiba Y, Inoue K, Kaji K, Cho K, Otsuki K (2008) Spatial variations in xylem sap flux density in evergreen oak trees with radial-porous wood: comparisons with anatomical observations. Trees 22(1):23–30. https://doi.org/10.1007/s00468-007-0165-8

Treanor NB (2015) China's Hongmu Consumption Boom: Analysis of the Chinese Rosewood Trade and Links to Illegal Activity in Tropical Forested Countries. Tech. rep, Forest Trends

Tu LY, Brennan JN, Sauer JA (1955) Dispersion of ultrasonic pulse velocity in cylindrical rods. J Acoust Soc Am 27(3):550–555. https://doi.org/10.1121/1.1907961

Ugochukwu AI, Hobbs JE, Phillips PW, Kerr WA (2018) Technological solutions to authenticity issues in international trade: the case of CITES listed endangered species. Ecol Econ 146:730–739. https://doi.org/10.1016/j.ecolecon.2017.12.021

Van Heerden FR, Brandt EV, Roux DG (1980) Isolation and synthesis of trans- and cis-(-)-clovamides and their deoxy analogues from the bark of *Dalbergia melanoxylon*. Phytochemistry 19(10):2125–2129. https://doi.org/10.1016/S0031-9422(00)82207-4

Varnier M, Sauvat N, Ulmet L, Montero C, Dubois F, Gril J (2020) Influence of temperature in a mass transfer simulation: application to wood. Wood Sci Technol 54:943–962. https://doi.org/10.1007/s00226-020-01197-y

Wenbin H, Xiufang S (2013) Tropical Hardwood Flows in China: Case Studies of Rosewood and Okoumé. Tech. rep, Forest Trends

Yang T, Zhou H, Ma E, Wang J (2018) Effects of removal of different chemical components on moisture sorption property of Populus euramericana Cv. under dynamic hygrothermal conditions. Results Phys 10:61–68. https://doi.org/10.1016/j.rinp.2018.05.024

Yin X, Huang A, Zhang S, Liu R, Ma F (2018) Identification of three Dalbergia species based on differences in extractive components. Molecules 23(9):2163. https://doi.org/10.3390/molecules23092163

Zadro MG (1975) Woods used for woodwind since the 16th Century 2: a descriptive dictionary of the principal woods mentioned. Early Music 3(3):249–251

Zelinka SL, Glass SV, Jakes JE, Stone DS (2016) A solution thermodynamics definition of the fiber saturation point and the derivation of a wood-water phase (state) diagram. Wood Sci Technol 50(3):443–462

Affiliations

Ahmad Alkadri[1,2] · Delphine Jullien[2] · Olivier Arnould[2] · Eric Rosenkrantz[3] · Patrick Langbour[4] · Louise Hovasse[1] · Joseph Gril[5]

Joseph Gril
joseph.gril@cnrs.fr

1 Henri Selmer Paris, 25 rue Maurice Berteaux, 78711 Mantes-la-Ville, France

2 Laboratoire de Mécanique et Génie Civil (LMGC), Université de Montpellier, CNRS (UMR 5508), Montpellier, France

3 Institut Électronique du Sud (IES), Université de Montpellier, CNRS (UMR 5214), Montpellier, France

4 BioWooEB Research Unit, CIRAD, TA B-114/16, 73 rue Jean-François Breton, 34398 Montpellier, France

5 CNRS, Sigma Clermont, Institut Pascal, Université Clermont Auvergne, Clermont-Ferrand, France